Soil deformation around a displacement pile in sand

D. J White & M. D. Bolton
Cambridge University Engineering Department

ABSTRACT: The observed unreliability in pile design methods suggests that the governing behaviour is not well understood. There is no consensus for the mechanism by which a pile penetrates sand or the soil properties which govern this behaviour. This paper presents some results of an investigation conducted to address this uncertainty. A plane strain calibration chamber is used to simulate the installation of a displacement pile. Particle Image Velocimetry (PIV) image analysis and close range photogrammetry allow the soil deformation during installation to be quantified to a high precision. Displacement and strain paths of soil elements close to the pile are presented for tests on carbonate and silica sands. The large shear and volumetric strains, and changes in principal strain direction during pile installation are quantified. Since the application of a working load to a displacement pile represents a reload stage after the installation process, the influence of the installation-induced strain paths on the serviceability behaviour of the pile is highlighted.

1 INTRODUCTION

1.1 Predicting pile behaviour

The axial capacity of displacement piles in sand is arguably the subject of greatest uncertainty in geotechnical engineering (Randolph et al. 1994). The most widely used technique for the design of long offshore displacement piles is that proposed by the American Petroleum Institute (API RP2A 1993). However, a large variation in $Q_{predicted}/Q_{measured}$ is exhibited by this method when compared to a comprehensive database of load tests (Jardine & Chow, 1996). For base resistance in sand, the API method exhibits a Coefficient of Variation (COV) (defined as the standard deviation, s, of $Q_{predicted}/Q_{measured}$ divided by the mean, μ) of 0.79.

1.2 Governing properties of base resistance in sand

The observed unreliability in pile design methods suggests that the governing behaviour is not well understood. There is no consensus for the mechanism by which a pile penetrates sand and the soil properties which govern this behaviour.

A number of approaches exist for predicting the base resistance of piles in sand. Analyses that use slip planes and bearing capacity theory to link friction angle with base resistance do not capture the trends observed in the field (Randolph et al. 1994).

Empirical methods (eg. API RP2A 1993) based on soil type and relative density and more advanced cavity expansion methods (eg. Randolph et al. 1994) have replaced the use of bearing capacity theory. However, these methods also exhibit significant unreliability (Jardine & Chow 1996), indicating that the correct link between soil properties and base resistance has not yet been identified.

Improved reliability can be achieved by using CPT data instead of soil properties for design. This bypasses the need to assume a penetration mechanism. By linking base resistance, q_b, to CPT resistance, q_c, Jardine & Chow (1996) obtain a reliability of COV= 0.20. This is achieved by incorporating a scale effect in which q_c is factored down by the ratio $[1- 0.5 \log (D/D_{cpt})]$.

This scale effect was attributed to the influence of shear banding, although no variable relating to shear band formation is included in the scaling factor. A qualitative explanation for this scale effect is that a dilating shear band will impede the penetration of a small CPT more than a large pile (Chow 1996). This hypothesis is plausible for a dense dilatant soil, but breaks down when extended to a loose or contractile soil. Either no scale effect will exist (if it assumed that shear banding will not occur in a strain-hardening material) or the opposite scale effect will exist (because a contracting shear band will ease the penetration of a small CPT more than a large pile).

Interaction between the stress fields created at the shaft and the base, which offers an alternative explanation for the base resistance scale effect (Borghi et al. 2001), is observed in the laboratory (Kezdi 1964, Hanke 2001, Eigenbrod et al. 2001) but not explicitly accounted for in any design methods.

This paper describes an investigation into the mechanism of pile penetration conducted to address the uncertainties described above. The investigation aims to clarify the kinematics of displacement pile installation, allowing the relevant regime of soil behaviour to be identified.

2 EXPERIMENTAL METHODOLOGY

2.1 Calibration chamber

Calibration chambers are widely used to study penetration resistance (eg. Houlsby & Hitchman 1988, Salgado et al. 1997, Yasufuku & Hyde 1995). The stresses and deformations around the tip of an advancing CPT or pile can be correctly replicated by applying a surcharge pressure at the boundary of the chamber. In order to observe the deformation around an advancing pile, a plane strain chamber with observation windows has been constructed (Fig. 1). Sheets of glass are placed on the inner faces of the box to reduce side friction. A surcharge pressure is applied to the top surface through a rubber bag. The model pile is jacked into the chamber at a rate of 1 mm/minute. Digital cameras are used to record images of the soil and pile at regular intervals.

Base resistance is measured using a total stress cell within the tip of the model pile. A total stress cell in the base of the box and a pressure transducer connected to the surcharge bags measure boundary stresses. Due to constraints of space, this paper will not discuss the measurements of stress, but will concentrate on the displacement and strain measurements obtained by photography through the main observation window.

2.2 Displacements from images

A novel technique for the non-contact measurement of soil deformation in physical models has been developed. This system combines digital photography, close-range photogrammetry and image analysis using Particle Image Velocimetry (PIV). Soil displacements are measured to a high precision without requiring intrusive target markers to be installed in the soil (Fig. 2).

Image processing algorithms based on PIV have been written to track the movement of small patches of soil (typically 2 - 4 mm in size) through a series of digital images to a precision of 1/15th of a pixel (White et al. 2001a). The images presented in this paper were captured using a Kodak DC280 digital camera, with a pixel resolution of 1760 x 1168.

Having measured the image-space coordinates of the deforming soil using PIV, these coordinates must be converted into model-space. This process is known as camera calibration. The calibration routine developed in this research uses 18 parameters to describe the model-space to image-space transformation. The PIV-photogrammetry system has a measured precision of 1/15000th of the field of view (White et al. 2001b).

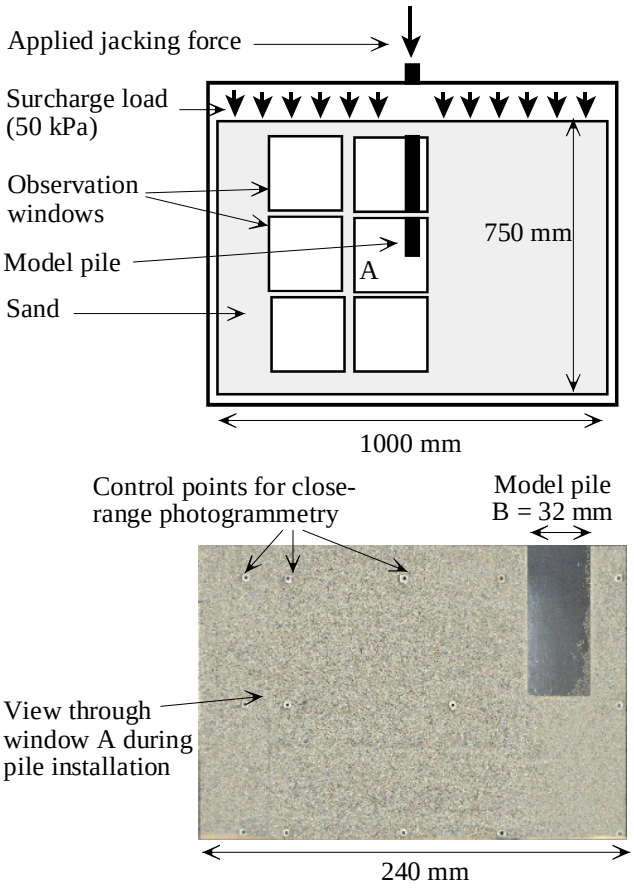

Figure 1. Schematic diagram of calibration chamber.

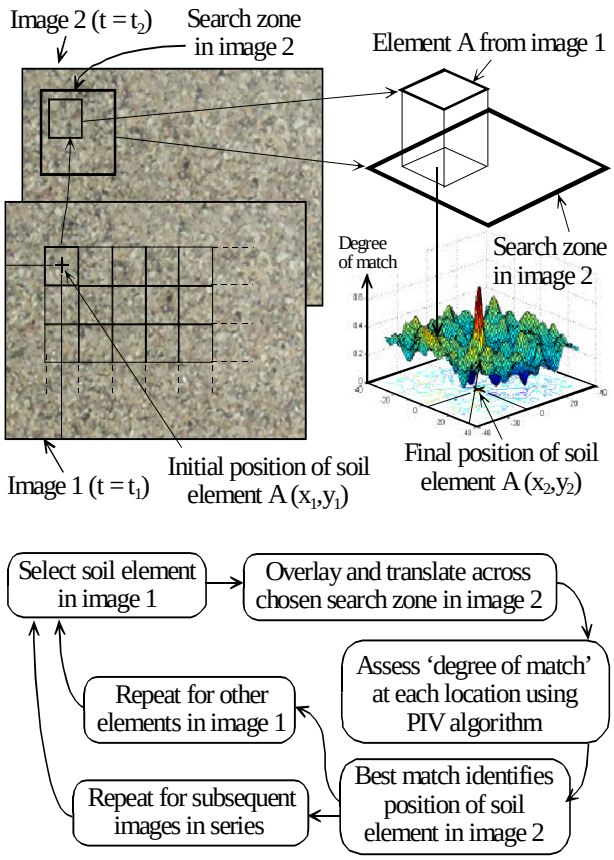

Figure 2. PIV analysis scheme.

2.3 Strains from displacements

Digital photographs of the pile and the surrounding soil are captured at 1mm intervals of penetration. This creates a sequence of approximately 400 images. In geotechnical modeling, this type of planar deformation is conventionally analysed by comparing of a single pair of images to construct an instantaneous field of displacement vectors. However, the gross deformations and curved displacement paths of soil around an advancing pile can be best quantified by analyzing the entire image sequence using PIV. Instead of plotting instantaneous displacement vectors, complete strain paths for each element of soil can be found.

A strain algorithm which detects rigid body rotation has been implemented. This is particularly important when evaluating strain paths in carbonate sand close to a pile. When deposited by pluviation, a highly anisotropic fabric is created by the elongated particles of Dog's Bay sand, and the flow around the pile tip includes significant rigid body rotation.

This strain algorithm operates on triangular elements of soil defined by a PIV patch at each corner. Strains at the centroid of each element are calculated by considering only the direct strains in each arm of the triangle, in a manner analogous to a strain gauge bridge. This approach avoids the calculation of shear strains from a single line element, which is numerically unstable if the line element is close to parallel with one of the reference directions. Linear strains have been used throughout this paper.

The reference axes are initially horizontal and vertical, but are allowed to rotate with the rigid body rotation of the soil element. As a result, the strain paths are plotted as experienced by the soil element. This allows the response to be compared with conventional element test data in which the soil element undergoes no rigid body rotation.

2.4 Model preparation

Results from two tests in dry sand are presented in this paper (Table 1). The mechanical properties of Dog's Bay sand are described by Coop (1990). Stroud (1971) and Lee (1990) present data for Leighton Buzzard fraction B silica sand. The soil models were prepared by air pluviation.

Test	Sand type	Voids ratio	Relative density
DJW02	Dog's bay carbonate	1.38	45%
DJW04	Leighton Buzzard Frac. B	0.70	20%

3 EXPERIMENTAL RESULTS

3.1 Penetration resistance

A surcharge pressure of 50 kPa was applied to the top surface of the soil model. The model pile was jacked to a depth of ≈400 mm. Steady state penetration at constant base resistance (q_b= 2 MPa ±2%) was reached in test DJW02 after a depth of ≈3B. In

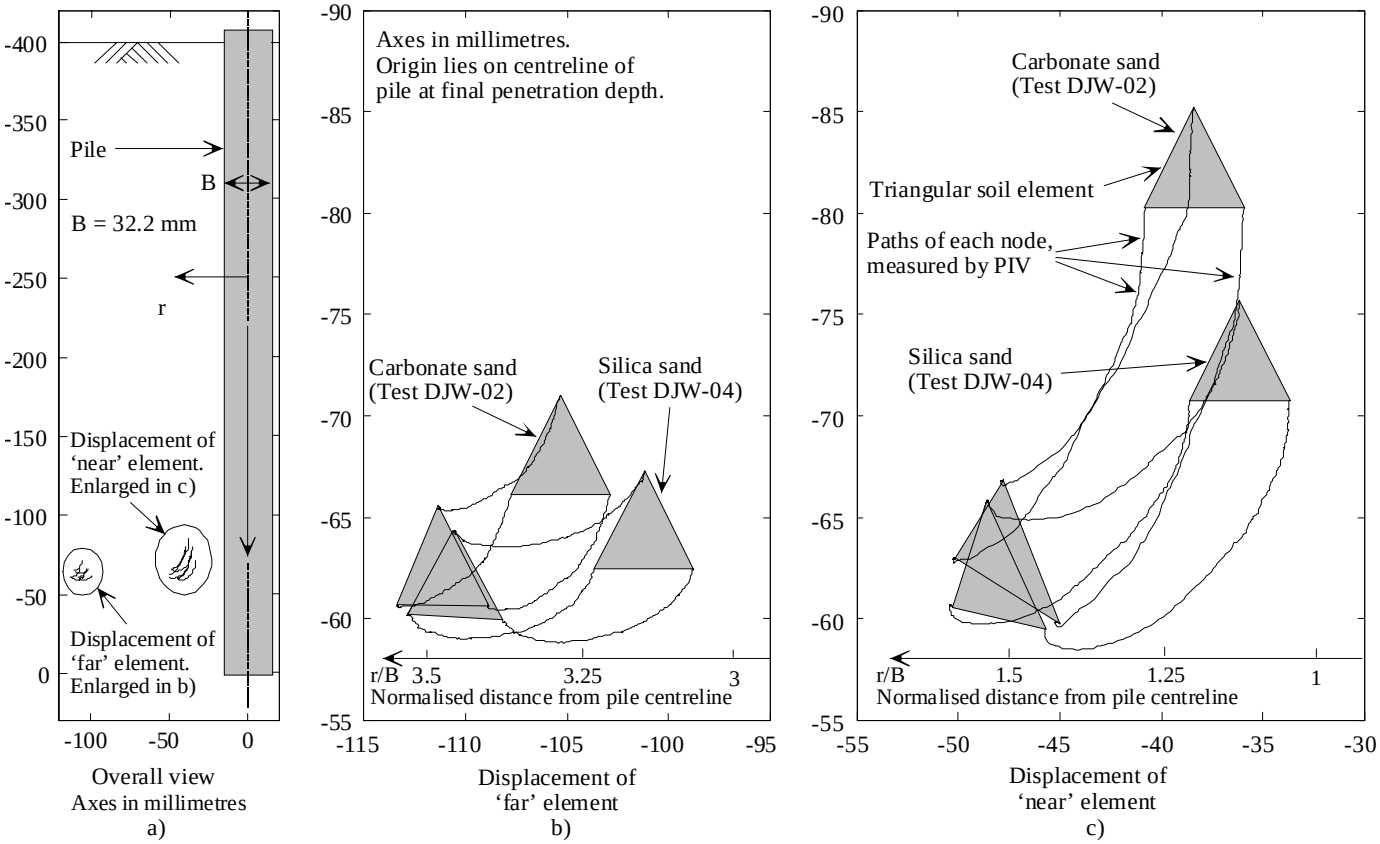

Figure 3. Displacement paths of 'near' and 'far' soil elements during pile installation.

test DJW04 an approximate steady state was reached, with q_b increasing slightly from 14 MPa to 17 MPa between 100 mm (≈3B) and 400 mm (≈12.5B) depth.

3.2 Displacement trajectories

The deformation of two triangular elements defined by PIV patches at each corner is presented in this paper. After installation of the model pile, these elements are located 1.5B and 3.5B from the centerline of the pile and 2B above the base, and are referred to as 'near' and 'far' respectively. The displacement paths of each element during installation are shown in Figure 3. Lateral displacement is observed, consistent with the idealization of pile installation as horizontal cavity expansion. Also, significant downward movement is observed in the near field.

3.3 Rigid body rotation

The rotation of each soil element evident in Figure 3 is quantified in Figure 4. The dimensionless distance h/B is used to illustrate the progressive deformation of each soil element as the pile approaches.

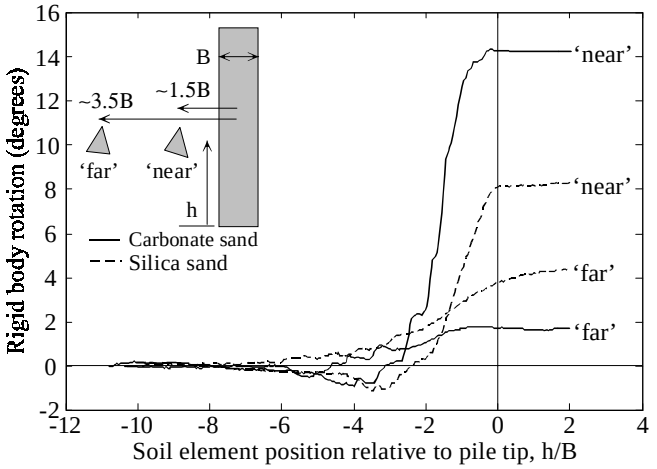

Figure 4. Rigid body rotation vs. pile position

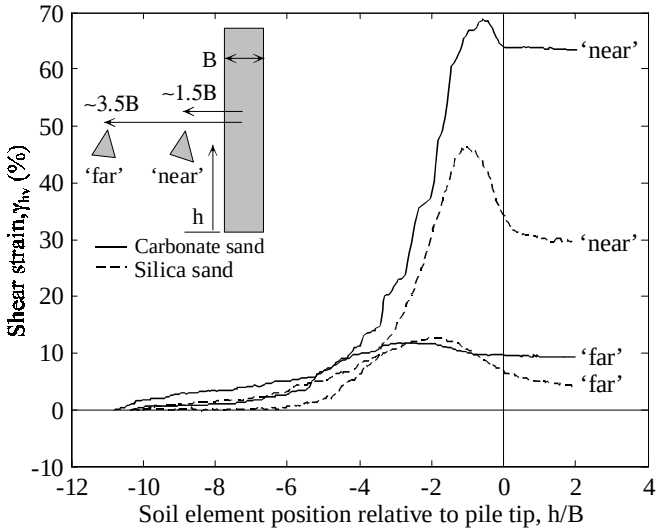

Figure 5. Shear strain vs. pile position

Noting that significant rigid body rotation is observed in the near field, the strain paths experienced by each soil element differ from those which would be deduced if rotation is ignored.

3.4 Shear and volumetric strain paths

Figures 5 and 6 show the shear and volumetric strains observed as the pile approaches and passes each element. The 'near' element undergoes strains which significantly exceed those seen in conventional element tests. Of note is the reversal in shearing direction which occurs just before the pile tip reaches the horizon of each soil element. This is followed by a small increase in volume of the 'near' element as the pile tip passes.

The lower shear and volumetric stiffness of the carbonate sand is evident. Although the base resistance in carbonate sand is ≈7 times lower than in silica sand, the observed shear and volumetric strains are approximately double. Figure 7 combines Figures 5 and 6 to illustrate the shear-volumetric strain paths, as would be observed in an equivalent element test.

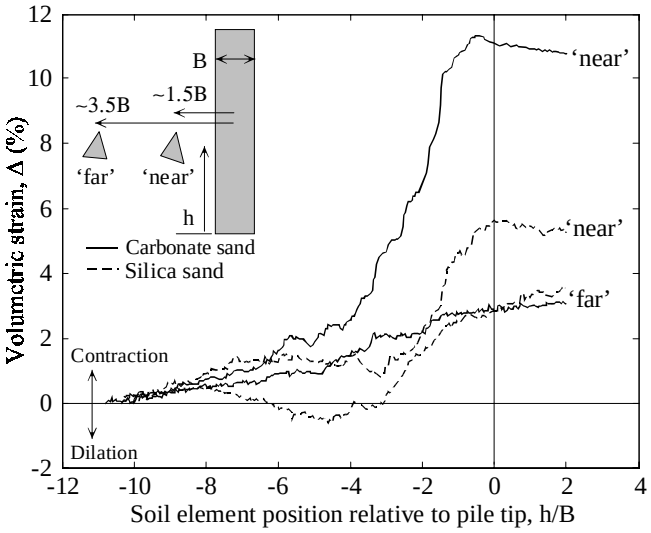

Figure 6. Volumetric strain vs. pile position

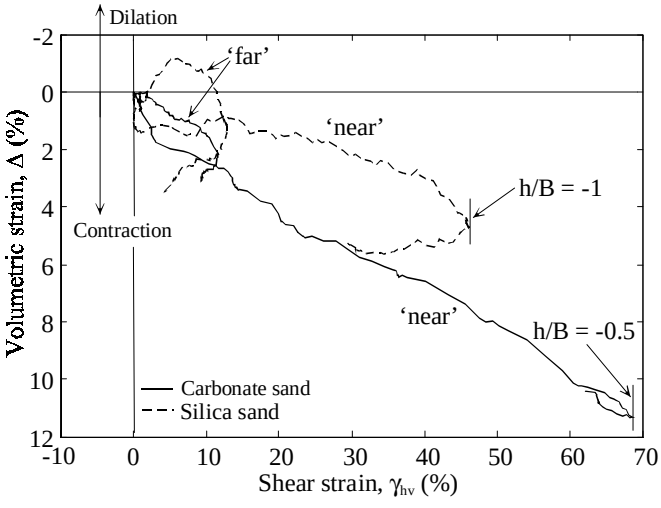

Figure 7. Shear strain vs. volumetric strain

However, plotting element deformation in shear-volumetric strain space hides any changes in strain direction. Whilst vertical (axial) and horizontal (radial) strains remain principal in a triaxial test, this is not the case during pile installation.

Since this investigation is conducted in plane strain, the deformation of each soil element can be considered as a biaxial element test. The biaxial strain path as the pile approaches can be illustrated by projecting a cross section through the evolving Mohr's circle of strain (Figs. 8 & 9). In this type of plot, the maximum and minimum principal strains form an envelope showing the boundary of the Mohr's circle. The maximum shear strain, γ_{max}, is equal to the width of this envelope.

In both the near and far fields, the out-of-plane strain of zero is always the intermediate principal strain, ε_{II}. The ε_I-ε_{III} envelope expands as shear strain accumulates before collapsing slightly as the pile passes and the direction of shearing reverses.

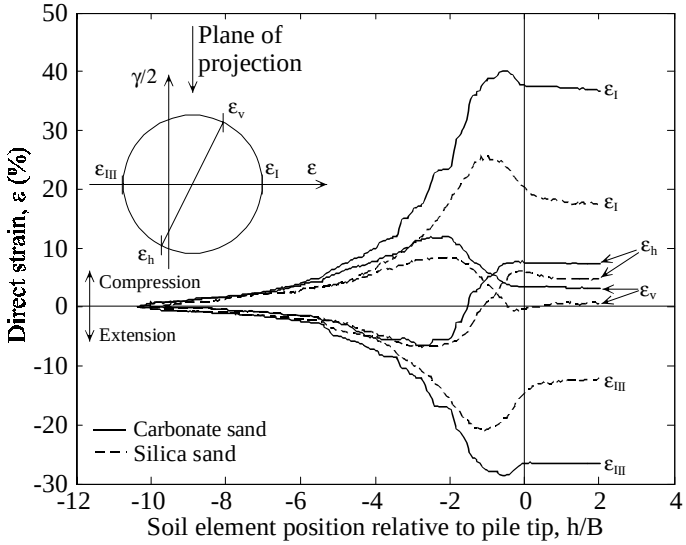

Figure 8. Projected Mohr's circles of strain: 'near' soil element.

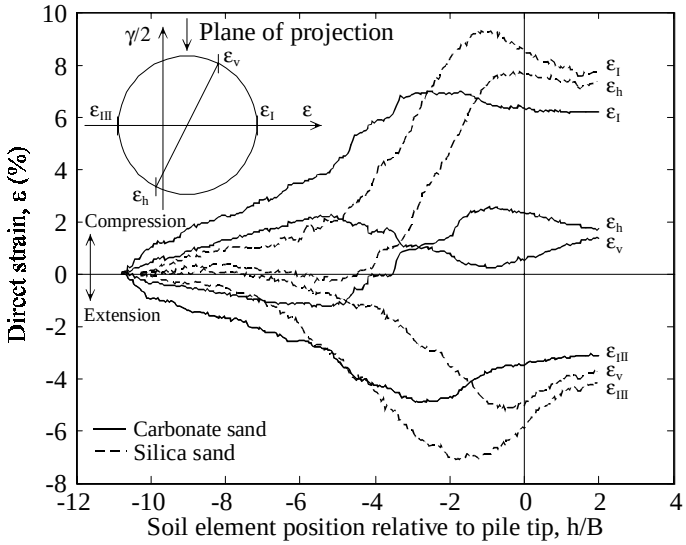

Figure 9. Projected Mohr's circles of strain: 'far' soil element.

Figure 8 shows that both vertical (ε_v) and horizontal (ε_h) strain in the 'near' element lie well within this envelope, indicating that neither are principal. ε_v and ε_h cross as the pile tip passes, indicating that the direction of straining reverses, accompanied by a rotation of the principal strain directions. Since ε_v and ε_h cross at the moment when the Mohr's circle is largest, the maximum shear strain experienced by the soil is in the h-v plane. This rotation of principal strain matches the likely rotation in principal stress as the soil element moves from vertically below the pile tip to horizontally adjacent.

In the far field (Fig. 9) different behaviour is observed in the two sands. In contrast to the near field, the maximum shear strain in the carbonate sand is *lower* than in the silica sand, demonstrating that in a compressible soil the installation process has a smaller zone of influence. Also, the strain directions are different; in silica sand, ε_v and ε_h are almost principal, whereas in carbonate sand they are close to planes of maximum shear strain.

4 DISCUSSION

4.1 Strain measurement

Previous physical modeling of displacement pile installation has allowed overall soil displacements to be deduced by comparing the initial and final positions of embedded markers (eg. Randolph et al. 1979). By using PIV, this investigation has been able to discard embedded markers and improve precision. As a result, displacement *paths* can be deduced, and differentiated to produce strain paths.

Controlled testing of the measurement system indicates a precision of approximately 1/15000th of the field of view (White et al. 2001b), which matches closely with the noise of 10 μm on the displacement measurements found in this investigation (Fig. 3).

4.2 Stress and strain regimes

The strain regime observed during the two tests described in this paper can be summarized as follows:

Soil element →	DJW02		DJW04	
Quantity ↓	'near'	'far'	'near'	'far'
Max. shear strain, γ_{max}	69 %	12 %	48 %	13 %
Plane of γ_{max}	h-v	h-v	h-v	20° to h-v
Max. volumetric strain	11%	3 %	6 %	3 %
Rigid body rotation	14°	2°	8°	4°

Table 2. Summary of strain paths

The near field strain path is characterized by shearing on vertical and horizontal planes accompanying vertical compression with horizontal extension followed later by horizontal compression and vertical extension. In both sands, the level of volumetric strain is sufficient to take the sand far enough down

an isotropic compression line to cross to the wet side of published critical state lines (Coop 1990, Stroud 1971). Furthermore, the maximum shear strain is sufficient to reach a critical state, including the test in Dog's Bay carbonate sand for which strains greater than >40 % can be required to reach the CSL (Coop 1999). Noting that the observed behaviour is characterised by features of CS behaviour, there may be opportunities to better capture pile capacity in sand using a critical state framework, as also suggested by Klotz & Coop (2001).

The far field strain path in carbonate sand follows the same trends as the near field, but with a six-fold reduction in shear strain. In silica sand the behaviour is different. The strain path is characterized by horizontal compression and vertical extension, with the major principal strain direction rotating towards the horizontal as the pile approaches.

4.3 Initial conditions for working load

The complex strain paths shown in this paper represent the installation process of a displacement pile. After installation, the pile will be under a working load significantly smaller than that applied during installation. The end points of these strain paths represent the initial conditions for the response of the pile to a working load. For design purposes, it is the soil properties present at the end of these strain paths which will govern the pile behaviour, rather than the in situ properties of the soil prior to pile installation.

Noting that in onshore applications it is usually the serviceability state which is critical in design (Randolph 1994), the relevant stiffness for a design calculation is the stiffness on reloading after the huge strain paths shown above (integrated in a suitable manner over the volume of soil around the pile).

5 CONCLUSIONS

The use of a plane strain calibration chamber combined with PIV image analysis has allowed a new insight into soil deformation during installation of a displacement pile. The deformation of two soil elements at different distances from the pile shaft is presented, and strain paths are revealed.

These strain paths represent the installation of a displacement pile, not the loading to failure. The subsequent application of the working load, has the end of the installation procedure as its initial conditions. Hence, the soil properties which govern the behaviour under working load are those present at the end of the strain paths shown in this paper.

6 ACKNOWLEDGEMENTS

The authors would like to thank Dr Adrian Hyde of the University of Sheffield for supplying the Dog's Bay sand, and Chris Collison and his team for their technical support throughout this work.

7 REFERENCES

American Petroleum Institute (API). 1993. RP2A: Recommended practice of planning, designing and constructing fixed offshore platforms- Working stress design, 20th edition, Washington 59-61.

Borghi, X., White, D.J., Bolton, M.D. & Springman S. 2001. Empirical pile design based on CPT results: an explanation for the reduction of unit base resistance between CPTs and piles. *Proc. 5th International Conference on Deep Foundation Practice, Singapore*. 125-132.

Chow, F.C. 1996. Investigations into the behaviour of displacement piles for offshore foundations, PhD thesis, Imperial College, U.K.

Coop, M.R. 1990 The mechanics of uncemented carbonate sands. *Géotechnique* 40(4): 607-626.

Coop, M.R. 1999. The influence of particle breakage and state on the behaviour of sands *International Workshop on Soil Crushability, Yamaguchi, Japan* 19-57,

Eigenbrod, K.D., Hanke, R., Phillips, R., Ip, S. & Basheer, M.A.J. 2001 Interaction between end bearing and shaft resisytance of piles. *Proc. 54th Can. Geotech. Conf. Calgary*

Hanke, R. 2001. Shaft capacities of close ended piles under load reversals in sand. MEng thesis Memorial University, St John's, Newfoundland

Houlsby, G.T. & Hitchman, R. 1988. Calibration chamber tests of a cone penetrometer in sand. *Géotechnique* 38(1): 39-44.

Jardine R. J. & Chow F. C. 1996. New design methods for offshore piles. *MTD Publication 96/103,* Marine Technology Directorate, London

Klotz, E. U. & Coop, M. R. 2001. An investigation of the effect of soil state on the capacity of driven piles in sands *Géotechnique* 51(9):733-751

Lee, S.Y. 1990. Centrifuge modelling of cone penetration testing in cohesionless soils. PhD thesis, Cambridge University.

Randolph, M.F., 1994. Design methods for pile groups and piled rafts *Proc. 13th International Conf. on Soil Mechanics and Foundation Engineering, New Delhi* (5):61-82

Randolph, M. F., Dolwin, J. & Beck, R. 1994. Design of driven piles in sand *Géotechnique* 44(3):427-448

Randolph, M.F., Steenfelt, J.S. & Wroth C.P. 1979. The effect of pile type on design parameters for driven piles. *Proc. 7th European Conference on Soil Mechanics and Foundation Engineering, Brighton* (2):107-114.

Stroud, M.A. 1971. The behaviour os sand at low stress level in the simple shear apparatus. PhD thesis, Cambridge University, UK.

Salgado, R., Mitchell, J.K. & Jamiolkowski, M. 1997. Cavity expansion and penetration resistance in sand. *ASCE Journal of Geotechnical and Geoenvironmental Engineering* 123(4): 344-354.

White, D.J., Take, W.A, Bolton, M.D. 2001a. Measuring soil deformation in geotechnical models using digital images and PIV analysis. *Proc. 10th Int. Conf. on Computer Methods and Advances in Geomechanics. Tucson, Arizona*. 997-1002 Balkema: Rotterdam.

White, D.J., Take, W.A, Bolton, M.D. & Munachen, S.E. 2001b. A deformation measuring system for geotechnical testing based on digital imaging, close-range photogrammetry, and PIV image analysis. *Proc. 15th Int. Conf. on Soil Mechanics and Geotechnical Engineering. Istanbul, Turkey*. (1):539-542. Balkema: Rotterdam.

Yasufuku, N. & Hyde, A.F.L. 1995. Pile end-bearing capacity in crushable sands. *Géotechnique* 45(4): 663-676.